Pergamon

PII S0016-7037(97)00049-5

SIMS analyses of minor and trace element distributions in fracture calcite from Yucca Mountain, Nevada, USA

RHAWN F. DENNISTON,[1,*] CHARLES K. SHEARER,[1] GRAHAM D. LAYNE,[1,†] and DAVID T. VANIMAN[2]

[1]Institute of Meteoritics, Department of Earth and Planetary Science, University of New Mexico, Albuquerque, New Mexico 87131, USA
[2]Earth and Environmental Science Division (EES-1), Los Alamos National Laboratories, Los Alamos, New Mexico 87545, USA

Abstract—Fracture-lining calcite samples from Yucca Mountain, Nevada, obtained as part of the extensive vertical sampling in studies of this site as a potential high-level waste repository, have been characterized according to microbeam-scale (25–30 μm) trace and minor element chemistry, and cathodoluminescent zonation patterns. As bulk chemical analyses are limited in spatial resolution and are subject to contamination by intergrown phases, a technique for analysis by secondary ion mass spectrometry (SIMS) of minor (Mn, Fe, Sr) and trace (REE) elements in calcite was developed and applied to eighteen calcite samples from four boreholes and one trench. SIMS analyses of REE in calcite and dolomite have been shown to be quantitative to abundances <1 × chondrite. Although the low secondary ion yields associated with carbonates forced higher counting times than is necessary in most silicates, Mn, Fe, Sr, and REE analyses were obtained with sub-ppm detection limits and 2–15% analytical precision.

Bulk chemical signatures noted by Vaniman (1994) allowed correlation of minor and trace element signatures in Yucca Mountain calcite with location of calcite precipitation (saturated vs. unsaturated zone). For example, upper unsaturated zone calcite exhibits pronounced negative Ce and Eu anomalies not observed in calcite collected below in the deep unsaturated zone. These chemical distinctions served as fingerprints which were applied to growth zones in order to examine temporal changes in calcite crystallization histories; analyses of such fine-scale zonal variations are unattainable using bulk analytical techniques. In addition, LREE (particularly Ce) scavenging of calcite-precipitating solutions by manganese oxide phases is discussed as the mechanism for Ce-depletion in unsaturated zone calcite. *Copyright © 1997 Elsevier Science Ltd*

1. INTRODUCTION

The origin of fracture-lining calcite deposits at the potential high-level radioactive waste repository at Yucca Mountain, Nevada, USA has been the subject of debate for the past several years. Most of this discussion has centered around whether or not these minerals are the result of typical near-surface (pedogenic) processes or were instead precipitated from tectonically-driven, upwelling groundwater (Broad, 1990; Marshall, 1991). Numerous studies aimed at resolving this controversy have produced data which convincingly support the pedogenesis model (Quade and Cerling, 1990; Stuckless et al., 1991; Peterman et al., 1992; Whelan and Stuckless, 1992; Vaniman, 1994). In addition to answering this question, bulk chemical analyses of fracture-lining calcite suggest that minor and trace element abundances in this calcite reflect conditions of precipitation. Previous research by Peterman et al. (1992), Whelan and Stuckless (1992), and Vaniman (1993, 1994) has demonstrated that fracture calcite from Yucca Mountain exhibit a variety of distinctly different chemical and isotopic signatures. These signatures are generally correlated to location within the site (e.g., deep saturated zone vs. upper unsaturated zone) and are thought to reflect the source of the calcite-precipitating

water, water chemistry, fluid/rock ratio, crystallization kinetics, or phases that precipitated prior to or along with the calcite. For example, upper unsaturated zone calcite may be differentiated from deep saturated zone calcite on the basis of (1) lower abundances of transition metals such as Fe and Mn relative to deep saturated zone calcite, (2) a pronounced negative Ce anomaly present only in upper unsaturated zone samples (with the exception of a small number of anomalous, shallow saturated zone calcite), and (3) a more prominent negative Eu anomaly in upper unsaturated zone calcite than in deep saturated zone occurrences (Vaniman, 1994).

Cathodoluminescence (CL) studies of this calcite reveal extensive and intricate zoning (on the scale of microns) reflecting a record of both continuous and discontinuous calcite growth (Denniston et al., 1993, 1994a, 1994b). These observations indicate that any bulk sampling method represents significant time-averaging of calcite precipitation events. Therefore, fine-scale precipitation events that reflect dramatic deviations in the source of water, water chemistry, crystallization kinetics, or other conditions of precipitation could very well be concealed by bulk analyses.

The micron-scale resolution offered by ion-probe in situ microanalysis may circumvent this and other problems such as contamination by intergrown opal, clays, and manganese oxides. While the use of ion-probe techniques for trace element analysis of carbonates has been shown to be very promising (Veizer et al., 1987; Swart, 1990; Savard et al., 1995), analysis of REE in carbonates has at best been qualitative.

---

* *Present address*: Department of Geology, University of Iowa, Iowa City, Iowa 52242, USA.
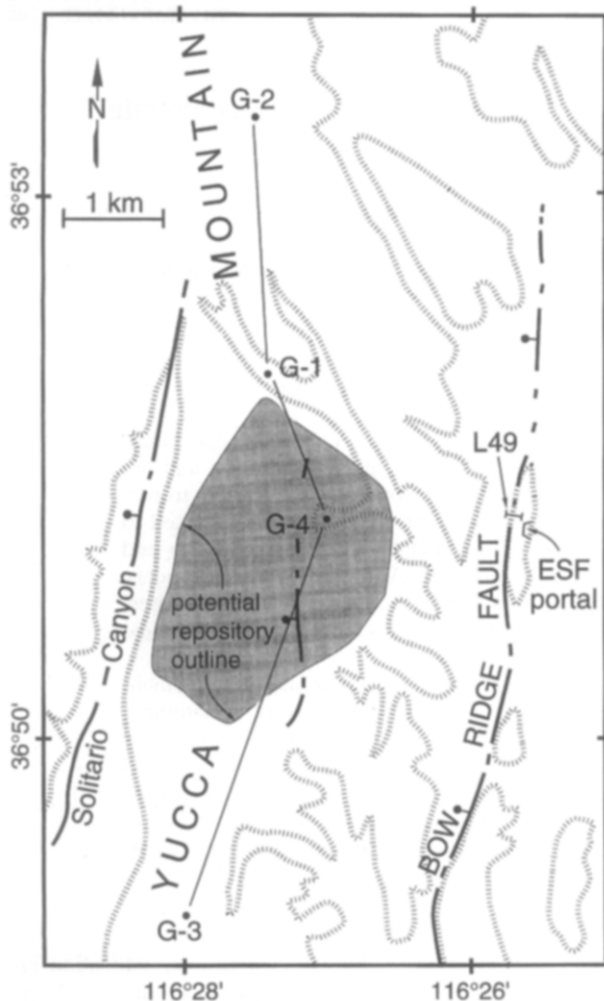† *Present address*: Woods Hole Oceanographic Institute, Woods Hole, Massachusetts, USA.

Fig. 1. Map of Yucca Mountain showing location of potential repository and the boreholes and trench used to obtain samples for this study.

The purpose of this research was to (1) develop precise and accurate methodologies for the analysis of REE, Mn, Fe, and Sr in carbonates by secondary ion mass spectrometry (SIMS); these include the identification and documentation of necessary homogeneous carbonate standards, (2) document the characteristics of growth zones in calcite from Yucca Mountain as defined by CL and trace/minor element characteristics, and (3) utilize trace element characteristics of growth zones in calcite to determine small-scale, temporal changes in crystallization conditions and to infer the possible conditions that may have lead to these changes.

2. GEOLOGIC AND HYDROLOGIC SETTING

Yucca Mountain is part of a prominent series of north-trending, fault-block ridges dipping predominantly eastward that extend from Beatty Wash in the northwest to U.S. Highway 95 in the Amargosa Desert (Fig. 1), an intermontane basin in the western Basin and Range. High-angle, extensional faults characteristic of the Basin and Range dominate regional topography. The area is underlain by highly folded

and faulted Early Paleozoic rocks. Pliocene sediments are the predominant basin fill (Hay et al., 1986).

Yucca Mountain is underlain by over 2200 m of Miocene silicic volcanic rocks associated with the Timber Mountain-Oasis Valley caldera complex. This volcanic series consists primarily of four major ash-flow tuffs. These include, in descending order, the (1) Paintbrush Group, which includes the Topopah Spring and Tiva Canyon tuffs, (2) the Calico Hills Formation, a nonwelded sequence of rhyolitic ash-flow tuff and bedded tuffs, (3) the Crater Flat Group, consisting of the Prow Pass, Bullfrog, and Tram rhyolitic ash-flow tuffs, and (4) the Lithic Ridge Tuff (Fig. 2). The potential location for a waste repository is in the upper unsaturated zone, most probably within the Topopah Spring Tuff. Stratigraphic designations based on drill-hole and surface studies are summarized in Sawyer et al. (1994).

A variety of calcite is found in the silicic tuffs of Yucca Mountain, Nevada. The soil zone and the upper 15m of tuff typically contain siliceous calcretes, fine-grained intergrowths of calcite and opal (Vaniman, 1994). Coarser-grained calcite spar, often associated with opal and/or zeolites and less commonly with other minerals (manganese oxides, chain-structure clays, kaolinite, and fluorite) occurs from ~15 m through deeper tuffs of the upper unsaturated zone (UUZ), down to 500 m. Here calcite is found in open and closed fractures, breccia zones, lithophysal cavities, and penetrating the tuff matrix (Vaniman, 1993, 1994). The carbonate-altered zone (CAZ) lies within the deep saturated zone at depths greater than 1 km. This area is characterized by tuffs and lavas altered to carbonate-bearing assemblages with chemically and texturally distinct Mn-rich calcite. The shallower part of this zone is characterized by analcime + calcite assemblages, while albite + calcite predominates at greater depths (Bish and Chipera, 1989). The barren zone (BZ), an area low in calcite abundance relative to the UUZ and the CAZ, underlies the UUZ from approximately 100–300 m above to approximately 400 m below the water table (Vaniman and Chipera, 1996).

Manganese oxides line some fractures in densely welded vitric and devitrified tuff throughout Yucca Mountain; the mineralogy and crystal form of manganese oxides appear to be broadly related to location above or below the water table (Carlos et al., 1993). For example, rancieite occurs primarily in the Paintbrush Tuff both above and below the water table, and cryptomelane is found predominantly in the saturated zone. Other manganese oxides include aurorite, lithiophorite, pyrolusite, and todorokite (Carlos et al., 1993). Relations in hand-sample suggest that manganese oxides typically predate calcite deposition (Carlos et al., 1993), although occurrences of pyrolusite intergrown with and postdating calcite have been found (Vaniman and Chipera, 1996).

The regional groundwater system in this area is recharged from outcrops of Paleozoic carbonates or upland tuffs; discharge occurs at Ash Meadows in the Amargosa Desert and in Death Valley (Czarnecki and Waddell, 1984; Hay et al., 1986). The water table at Yucca Mountain lies approximately 500–700 m below the landsurface. The low permeability of the Topopah Spring and other lithologic units, coupled with the extensive accumulation of secondary minerals along faults and fractures, suggests that fractures and/
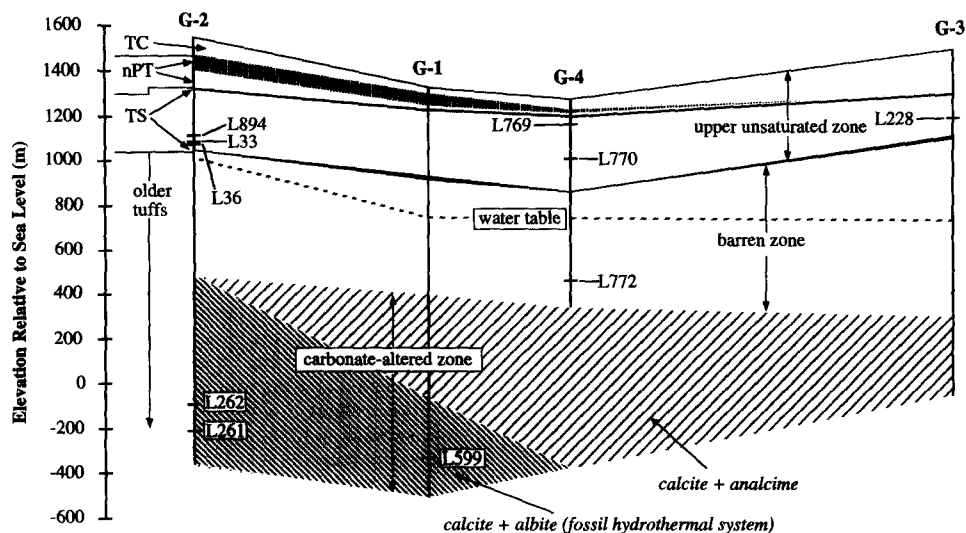
Fig. 2. Cross-section of Yucca Mountain including major lithologic units and sample locations with respect to boreholes, the water table, upper unsaturated zone, barren zone, and carbonate-altered zone. TC = Tiva Canyon Tuff; nPT = non-welded Paintbrush Tuff; TS = Topopah Spring Tuff.

or faults may be important fluid conduits. The presence of zeolitized areas immediately overlying the current water table and in isolated pockets in shallower locations throughout the unsaturated zone may delineate ancestral groundwater levels.

3. PREVIOUS RESEARCH

A great deal of the literature concerning secondary carbonate mineral formation at Yucca Mountain has focused on the variations in isotopic and chemical composition relative to local groundwater levels. These include comparisons of minor and trace element chemistries, stable isotope analyses, and fluid inclusion studies.

3.1. Previous Studies of Yucca Mountain Calcite

3.1.1. Stable/radioactive isotopes

Quade and Cerling (1990) noted that fine-grained calcretes at Yucca Mountain contained calcite with $\delta^{13}C$ and $\delta^{18}O$ signatures suggesting pedogenic origins, with formation occurring dominantly during cooler past climates. For coarser-grained calcite below the surface, Whelan and Stuckless (1992) demonstrated that $\delta^{13}C$ (PDB) values for unsaturated zone calcite (−9 to −3‰) are typically lower than calcite from the saturated zone (−2 to +3‰). Strontium isotopic studies by Peterman et al. (1992) support this distinction. They noted that while strontium isotopic signatures of saturated zone and deep unsaturated zone fracture calcite are very similar to those of their host tuffs, most $^{87}Sr/$ ^{86}Sr values of calcite located approximately 100 m above the current water table are decoupled from the Sr signatures of adjacent lithologies (Fig. 3). Peterman et al. (1992) suggest two possible explanations: (1) calcite precipitation during a higher position of the water table or (2) aqueous diffusion of Ca and Sr upward from the water table into a zone of partial supersaturation.

U-series dating of unsaturated zone samples provides evidence of calcite ages ranging from 26,000 to greater than 400,000 y, with major episodes of carbonate deposition occurring at 28, 170, and 280 ka. (Szabo and Kyser, 1990). Stuckless et al. (1991) obtained similar $^{234}U/^{238}U$ for Yucca Mountain soils and vein carbonates from Trench 14, reinforcing support for the pedogenic origin of these occurrences (Fig. 1).

3.1.2. Fluid inclusions

Fluid inclusion studies by Roedder et al. (1994) suggest formation temperatures for unsaturated zone calcite at or near current values and P_{O_2} and P_{N_2} at approximately atmo-
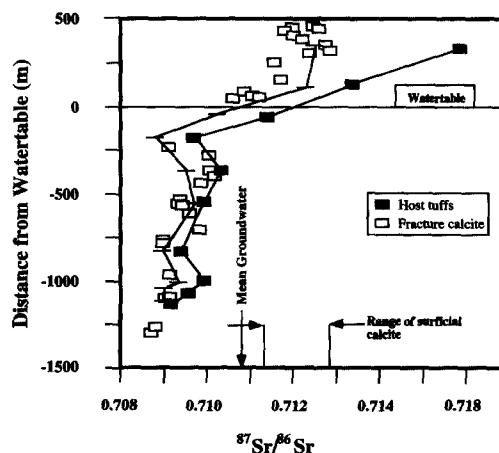

Fig. 3. Plot of $^{87}Sr/^{86}Sr$ values for fracture-filling calcite and volcanic rock vs. depth at Yucca Mountain. Note the divergence of the calcite tuff Sr signatures at approximately 100 m above the water table which may represent a past increase in groundwater levels. After Peterman et al. (1992).

spheric levels. Many CAZ calcite appear to have formed
during a low temperature (<250°C) hydrothermal event
probably associated with the Timber Mountain caldera event
at 10.4 Ma (Bish and Aronson, 1993).

3.1.3. Calcite chemistry

Vaniman (1993) noted that the pronounced negative Eu
and Ce anomalies present in UUZ calcite are not typical
of CAZ calcite (those associated with the albite-analcime
alteration). Instrumental neutron activation analyses
(INAA) of calcite + opal intergrowths from the soil zone
suggest that Ce anomalies may appear within the upper 3 m
of calcrete and are generally present in both calcrete and
calcite samples at depths exceeding 3 m (Vaniman and
Whelan, 1994). Vaniman (1993) also observed generally
lower abundances of transition metals (Fe, Mn, Sc) in UUZ
calcite relative to its CAZ counterparts.

3.1.4. Anomalous calcite

Scattered calcite samples collected from the UUZ (above
the level of analcime + calcite or albite + calcite alteration)
exhibit $\delta^{13}C$ and $\delta^{18}O$ signatures close to average unsaturated
zone values. These occurrences are compatible with younger
calcite derived from the Tertiary volcanic aquifer, or they
may have formed from deep infiltration of meteoric waters
at a point when groundwater levels were lower than present.
Similarities in strontium isotope composition were also ob-
served between some fracture-filling calcite in the 100 m
interval immediately above the water table and the mean
groundwater value from the Cenozoic aquifer (Peterman et
al., 1992). Also, $\delta^{13}C$ and $\delta^{18}O$ signatures similar to satu-
rated zone calcite were obtained from some unsaturated zone
calcite located up to approximately 400 m above the current
water table; Whelan and Moscati (unpubl. data) suggest that
this calcite may represent a very early calcite-forming event.

3.2. Previous SIMS Analysis of Calcite

Previous SIMS analyses of calcite have been limited in
number. Mason (1987) used SIMS to examine minor and
trace element (Mn, Fe, Sr, Mg) abundances and to constrain
the relationship between Fe/Mn ratios and CL in carbonifer-
ous limestone cements. Riciputi et al. (1992, 1994a) corre-
lated trace element (B, Na, Mg, Al, Fe, Mn, Sr, and Ba)
distributions in secondary and primary calcite and dolomite
to identify distinct diagenetic fluids that affected Devonian
carbonates. Srinivasan et al. (1994b) performed a similar
study of Cambro-Ordovician carbonates using select REE.
Riciputi et al. (1994) investigated B, Na, Mg, Fe, Mn, Sr,
and Ba concentrations in carbonates of carbonaceous chon-
drites. Veizer (1987) and Swart (1990) investigated the rela-
tionship among Sr, Mn, Fe, and Mg in calcite and dolomite
primarily to assess the effectiveness of the analytical tech-
nique. Most recently, Savard et al. (1995) analyzed Na, Mg,
Al, Si, Ca, Fe, Mn, Sr, Ba, and Ce in calcite using SIMS.
However, because Na, Al, Si, Ba, and Ce were not calibrated
against standards and were instead normalized to the pre-
dicted periodic nature of the ion yield, abundances deter-
mined for these elements are only order-of-magnitude esti-

mates. Although these previous studies illustrate the effec-
tiveness of using SIMS to analyze Sr, Mn, and Fe in
carbonates, the present study marks the first simultaneous,
quantitative SIMS analysis of REE, Mn, Fe, and Sr in car-
bonates.

4. ANALYTICAL TECHNIQUES

Research for this project was divided into two parts. The first
portion involved developing a technique for the simultaneous analy-
sis of Sr, Mn, Fe, and REE in calcite using SIMS. Quantification of
secondary ion intensities in SIMS requires the use of standards that
have major-element compositions similar to those of the unknowns,
because of matrix effects on ion yields (Shimizu et al., 1978; Riciputi
et al., 1994). In addition, ion intensities of the elements of interest
must be calibrated with ion intensities of an element of known
concentration in the sample (Riciputi et al., 1994). Bulk chemical
analyses of potential standards were obtained using inductively-cou-
pled plasma mass spectrometry (ICP-MS) and INAA, while chemi-
cal heterogeneity was assessed by CL, electron microprobe, and ion
microprobe techniques. Using ICP-MS, the chemistries of calcite
from a wide variety of terrains were investigated as potential SIMS
standards. Penn St., a calcite sample from the Oka carbonatite, and
CRC, from a Mexican hydrothermal deposit, were chosen as stan-
dards. Once suitable standards were identified, calibration curves
were constructed and isobaric interferences were investigated.

The second portion of this study involved the characterization and
analysis of fine-scale zoning in selected Yucca Mountain calcite.
This consisted of (1) sample photodocumentation, including correla-
tion of reflected light images with photomicrographs of CL zoning,
(2) electron microprobe analyses of minor and major element chem-
istries of zones and associated mineral phases, (3) ICP-MS analyses
of selected associated mineral phases (manganese oxides), and (4)
SIMS analyses of minor and trace element abundances in growth
zones.

4.1. Inductively-Coupled Plasma Mass Spectrometry (ICP-MS)

ICP-MS analyses of trace elements in potential carbonate stan-
dards and in manganese oxide phases associated with calcite at
Yucca Mountain were performed using a VG PQ2 ICP-MS. The
manganese oxides were analyzed in order to better constrain the
origin of a negative Ce anomaly associated with many unsaturated
zone carbonates. The carbonates and manganese oxides were dis-
solved in concentrated HCl at 110°C. Solutions were taken to com-
plete dryness. Samples were then redissolved in concentrated nitric
acid and brought up to 25 mL using deionized water. An In and Re
internal standard was added to the resulting solution. Analytical
accuracy and precision was better than 5% for the trace elements
analyzed in both the calcite and the manganese oxides.

4.2. Cathodoluminescence (CL)

Cathodoluminescence studies were conducted at Los Alamos Na-
tional Laboratory on a Nuclide Corporation Luminoscope, model
ELM2B, with an accelerating potential of 15 kV, beam current of
0.4 mA, focused beam diameters ranging from 1–5 mm, and residual
gas and chamber pressure of approximately 50 millitorr. Sample
chamber vacuum was maintained with a flow-through atmosphere
of research grade He. Photomicrographs of luminescing calcite were
predominantly obtained using 1600 ASA color film, with exposure
times varied to reflect luminescing qualities of each calcite and
fluctuations in beam current.

4.3. Electron Microprobe

Quantitative analyses of potential standards were obtained with a
JEOL 733 Superprobe operated by the Department of Earth and
Planetary Sciences at the University of New Mexico. This electron
microprobe is equipped with a backscattered electron detector, five
wavelength spectrometers, and an Oxford LINK eXL II operating
system. Analyses were conducted using a 15 kV accelerating voltage,

20 nA beam current, and beam diameter of 10–20 μm. Analyses were performed using high quality natural mineral standards (calcite for Ca, dolomite for Mg, siderite for Fe, spessartine for Mn, and celestite for Sr) and wavelength dispersive spectrometer peak counting times of 20 s for major and 30 s for minor elements. ZAF corrections were applied to all microprobe analyses. Analytical precision is a function of several factors including sample abundance of the elements of interest, but errors were typically less than 3% for major and 5% for minor elements.

Additional analyses were conducted in the Earth and Environmental Science Division of Los Alamos National Laboratory on a Cameca SX-50 electron microprobe. Operating conditions included a 15 kV accelerating potential, 15 nA beam current, and 10 μm beam diameter. PAP matrix corrections were applied to each analysis. For a more complete description of electron microprobe operating conditions see Vaniman (1994).

4.4. Secondary Ion Mass Spectrometry (SIMS)

Minor (Fe, Mn, Sr) and trace (REE) element analyses were performed by SIMS using the CAMECA IMS 4f instrument operated by the University of New Mexico/Sandia National Laboratories Ion Microprobe Facility. Each analysis involved repeated cycles of peak counting on ^{44}Ca$^+$, ^{55}Mn$^+$, ^{57}Fe$^+$, ^{88}Sr$^+$, ^{139}La$^+$, ^{140}Ce$^+$, ^{146}Nd$^+$, ^{147}Sm$^+$, ^{151}Eu$^+$, ^{153}Eu$^+$, ^{163}Dy$^+$, ^{167}Er$^+$, and ^{174}Yb$^+$, as well as counting on a background position to monitor detection noise. Software constraints limited the number of isotopes analyzed per cycle to thirteen. SIMS analyses were conducted by bombardment of the samples with primary O$^-$ ions accelerated through a nominal potential of 10 kV. A primary ion current of 20–40 nA was focused on the sample over a spot diameter of 25–30 μm. The locations of the analytical spots were selected using both reflected light and CL photomicrograph mosaics. Sputtered secondary ions were energy filtered using a sample offset voltage of -125 V and an energy window of 50 V to effectively eliminate isobaric interferences. Peak counting times were varied to achieve an analytical precision of at least 15% (typically 5–10%) on each element (Table 1).

The Cameca 4f is equipped with a computer system that allows automated control of magnetic peak switching, and peak positions were calibrated each day. These SIMS analyses were used in conjunction with CL and electron microprobe traverses to establish the homogeneity of the calcite standards. Prior to each analysis, sample areas surrounding the spot were cleaned with a rastered primary beam to eliminate contamination from the gold coat and surface layer of the sample. Spots were also pre-sputtered for approximately 1 min to allow secondary ion signals to stabilize. Following rastering and pre-sputtering, ten cycles of data were collected with total analysis times of 40–50 min.

The secondary ion spectrum contains oxides, dimers, and hydrides, as well as elemental ions that can complicate the collection of high precision, quantitative analyses. These interfering species can be effectively eliminated using energy filtering (Shimizu et al., 1978; Swart, 1990), high mass resolution (Mason, 1987), spectral stripping (Veizer et al., 1987; Mason, 1987), or analysis of double-charged ions (Riciputi et al., 1992). Energy filtering appears to be the most effective of these techniques for analyzing carbonates. The only prominent interference not corrected by this technique was ^{40}Ca^{16}O$^+$ on the ^{56}Fe$^+$ peak, but this was avoided by counting on the ^{57}Fe$^+$ peak. The effect of ^{135}Ba$^+$ and ^{137}Ba$^+$ interference on the Eu signal was monitored by looking for variations from natural abundance in ^{151}Eu$^+$ and ^{153}Eu$^+$, but absolute Ba concentrations were always too low to cause significant interferences with Eu. The three HREE analyzed in this study were chosen based on two criteria: (1) relative isotopic abundance ratios for each element and (2) the effects of interfering LREE-oxides.

Absolute concentrations of each element were calculated using empirical relationships between concentrations and measured peak/^{44}Ca$^+$ ratios, normalized to known CaO content, as derived from measurements of a documented standard (Shimizu et al., 1978). This relationship is shown by the following equation:

$$C_U = C_{std} \times [(IM_U/I^{44}Ca_U \times CaO_U)/(IM_{std}/I^{44}Ca_{std} \times CaO_{std})]$$

where

C_U = concentration of element in unknown
C_{std} = concentration of element in standard
$I^{44}Ca_U$ = intensity of ^{44}Ca signal in unknown
$I^{44}Ca_{std}$ = intensity of ^{44}Ca in standard
IM_{std} = intensity of analytical peak of element in standard
IM_U = intensity of analytical peak of element in unknown
CaO_U = abundance of CaO in unknown
CaO_{std} = abundance of CaO in standard

In constructing operation curves, isotope signals were normalized to ^{44}Ca$^+$ in order to avoid detector damage from the high ^{40}Ca$^+$ signal.

As previously reported by Mason (1987), secondary ion yields are considerably lower for calcite and dolomite than for silicate minerals. Lower yields translate to lower count rates. As the precision of an analysis is a function of the counts accumulated, counting times were longer for carbonates than for similarly enriched silicates. With the exception of Ce, REE in silicates typically ionize in a systematic fashion which allows a single calibration curve to include each element. However, individual REE in carbonates ionize with significantly different yields under primary ion bombardment, requiring separate calibration curves for each element.

The results of SIMS analyses of minor elements correspond well to those obtained using electron microprobe techniques. Electron microprobe detection limitations do not allow correlation between trace element analyses.

Dolomite was analyzed in only one sample, L261, a saturated zone calcite from borehole USW G-2. Comparisons of electron microprobe and SIMS analyses from one occurrence of dolomite in this section indicate that dolomite shares the low ionization potential of calcite, as noted by Mason (1987). Strong correlations between electron microprobe and SIMS analyses suggest that calibration curves constructed for Fe, Mn, and Sr in calcite are applicable to dolomite, suggesting that calibration curves for REE in calcite may also apply to dolomite. Swart (1990) also observed no significant differences in the calibration for calcite and dolomite with respect to Mg, Fe, Mn, and Sr.

5. RESULTS

5.1. Cathodoluminescence

Cathodoluminescence, the emission of light induced by electron bombardment of a phosphor, provided several benefits to this research but was primarily used as a means of quickly constraining chemical heterogeneity throughout an entire calcite sample. For the purpose of this research, luminescence refers only to visible wavelengths. Luminescence depends on impurities in crystalline structures that act as activators or quenchers (Long and Agrell, 1965). In carbonates, Mn^{2+} is the principle activator, while Fe^{2+} quenches luminescence (Long and Agrell, 1965; Nickel, 1978; Mason, 1987). The role of REE as activators of CL has also been demonstrated in a wide range of minerals, including calcite and dolomite in rare cases (Mason and Mariano, 1988; Mariano, 1989).

Luminescent zonation in Yucca Mountain UUZ calcite typically consists of 1–20 μm alternating luminescing and nonluminescing zone pairs. Many CAZ calcite samples exhibit similar, although broader (20–50 μm), oscillatory zoning (Fig. 4a). Irregularly shaped luminescing and nonluminescing zones (50–150 μm wide) and areas composed of randomly distributed patches (<5 μm) of luminescing calcite are also common in CAZ samples (Fig. 4b). Suture-form discontinuities between domains of such fine banding may mark a hiatus in calcite precipitation or differing traces

R. F. Denniston et al.

Table 1. Results of SIMS analyses. Fe in L599 by electron probe. BD = below detection. NA = not available. Data in ppm.

| Location, Sample & Analysis	CL: Dark (D), Light (L), or Both (B)	La	Ce	Nd	Sm	Eu	Dy	Er	Yb	Mn	Fe	Sr
					Soil Zone							
L49-1	D	BD	0.05	0.06	BD	BD	BD	BD	BD	0.58	15.2	51.9
L49-2	D	BD	BD	BD	BD	BD	BD	BD	BD	0.49	19.4	88.6
				Upper Unsaturated Zone								
L33-1	D, L	11.6	0.02	21.5	11.7	0.74	22.4	13.9	10.4	0.19	30.1	5.28
L33-2	B	0.99	BD	2.39	1.16	0.07	3.10	2.27	1.23	0.10	17.2	3.92
L33-3	D	0.54	BD	0.99	0.62	0.05	1.17	0.56	0.66	0.31	10.4	6.90
L36-1	D	9.24	0.25	16.4	7.13	0.40	15.8	9.59	7.16	0.10	13.1	2.11
L36-2	L	130	0.14	142	54.0	2.67	48.2	16.2	8.82	0.05	13.6	2.58
L36-6	D	11.3	0.05	11.3	6.74	0.50	26.8	12.0	7.55	0.25	6.57	3.95
L36-4	D	25.8	0.14	32.5	17.3	0.94	30.3	14.6	8.59	0.27	7.01	3.78
L36-5	L	230	0.12	230	87.0	3.97	60.9	16.5	8.99	0.08	9.16	2.28
L36-6	L	78.4	0.15	92.5	29.4	1.13	27.1	11.0	8.26	0.81	11.7	7.54
L36-7	D	3.77	0.11	7.71	4.90	0.35	14.5	7.71	4.12	0.09	5.73	1.84
L36-8	NA	20.7	0.16	21.4	12.2	0.83	33.5	20.3	10.3	0.32	112	4.25
L36-9	NA	25.3	0.36	39.6	19.4	1.14	46.8	27.8	14.4	0.38	14.9	2.82
L228-1	D	BD	BD	BD	BD	BD	BD	BD	BD	0.10	136	461
L228-2	D	BD	BD	BD	BD	BD	BD	BD	BD	BD	60.1	134
L228-3	D	BD	BD	BD	BD	BD	BD	BD	BD	0.07	71.4	265
L589-1	D	0.05	BD	BD	BD	BD	BD	BD	0.02	0.21	53.5	25.3
L589-2	D	BD	BD	BD	BD	BD	BD	BD	0.03	0.36	37.4	30.6
L589-3	D	0.02	BD	BD	BD	BD	BD	BD	0.09	0.06	37.9	159
L589-4	D	0.01	BD	BD	BD	BD	BD	BD	BD	0.06	14.0	80.4
L769-1	B/L	0.03	BD	0.109	BD	BD	BD	BD	BD	0.50	331	25.7
L769-2	B/L	0.58	0.02	0.92	0.12	0.03	0.08	BD	0.09	0.07	139	73.3
L770-1	B	2.66	0.01	7.00	2.68	0.06	5.07	3.58	3.56	0.05	247	167
L770-2	B	9.37	0.06	14.1	5.14	0.12	6.63	4.56	4.94	0.06	85.5	87.3
L770-3	B	20.8	0.05	39.3	17.0	0.30	14.8	8.95	8.18	0.05	66.3	142
L770-4	B	0.80	0.05	1.48	0.92	0.03	0.98	0.57	0.56	0.05	45.5	5.60
L770-5	NA	0.58	0.28	1.52	0.71	0.05	0.96	0.86	0.62	0.12	191	51.3
L887-1	D	41.5	0.12	63.8	22.4	0.94	11.4	5.42	3.98	0.58	64.3	149
L887-2	D	1.23	0.00	7.28	5.34	0.19	12.2	8.23	5.96	0.05	75.2	40.7
L887-3	D	1.08	0.00	3.47	1.68	0.11	4.68	3.03	1.79	0.06	62.1	132
L887-4	D	0.06	0.00	0.37	0.33	0.01	1.51	0.93	0.81	0.06	69.9	125
L887-5	D	11.4	0.03	50.2	29.9	1.09	45.4	24.9	16.4	0.05	30.0	51.0
L894-1	D	50	0.17	32.3	12.9	0.66	20.7	10.8	5.96	0.10	41.9	7.19
L894-2	D	3.5	BD	4.31	2.16	0.12	4.15	2.84	1.84	0.10	20.8	11.4
L894-3	NA	80.7	0.16	53.8	19.7	0.89	28.2	16.0	9.73	0.22	27.3	6.07
L894-4	NA	2.61	0.04	4.00	1.87	0.09	3.49	2.35	1.36	0.31	31.0	11.8
L990-1	D	0.02	0.33	BD	BD	BD	BD	BD	0.06	1.12	61.0	219
L990-2	D	0.13	0.02	BD	BD	BD	BD	BD	0.42	0.31	44.5	346
L990-3	D	0.11	0.02	0.16	0.09	0.03	0.29	0.29	0.24	0.26	27.3	398
L990-4	D	0.01	BD	BD	BD	BD	BD	BD	0.02	0.19	32.5	380
L1678-1	D	1.81	0.11	3.51	1.46	0.06	1.08	0.36	0.24	0.11	82.5	83.2
L1678-2	D	0.05	BD	BD	BD	BD	BD	BD	BD	0.05	97.0	83.3
L1678-5	D	3.50	0.00	3.37	0.96	0.04	0.61	0.37	0.16	0.04	29.2	60.6
L1896-1	D	34.5	0.68	31.4	10.2	0.2	14.6	9.79	8.14	0.41	88.5	153
L1896-3	D	55.1	1.24	46.1	14.6	0.3	19.8	15.2	12.0	1.05	77.1	180
L1896-4	D	3.89	0.67	2.76	0.67	0.02	1.43	1.12	0.80	13.0	29.7	66.4
L1897-1	D	0.11	BD	BD	BD	0.02	BD	BD	0.02	0.06	47.7	46.2
L1897-2	D	0.01	BD	BD	BD	BD	BD	BD	BD	0.10	43.3	71.4
L1897-3	D	0.00	0.04	BD	BD	BD	0.029	BD	0.05	0.05	78.6	42.9
L1897-6	D	0.71	BD	BD	BD	BD	BD	BD	0.35	0.07	31.2	36.5
L1897-7	D	0.37	0.01	0.68	0.26	0.01	0.32	0.27	0.16	0.05	177	39.2
L1898-1	D	BD	BD	BD	BD	BD	BD	BD	BD	0.07	38.7	9.64
L1898-2	D	0.11	BD	BD	BD	BD	BD	BD	0.21	0.18	32.5	2.38
L1898-3	D	0.04	BD	BD	BD	BD	BD	BD	0.05	0.09	24.5	6.11
L1898-4	D	0.01	BD	BD	BD	BD	BD	BD	BD	0.03	74.5	2.21
L1898-5	D	0.01	BD	BD	BD	BD	0.02	BD	BD	0.04	97.8	1.14
L1898-6	D	BD	BD	BD	BD	BD	BD	BD	BD	0.03	29.2	41.4
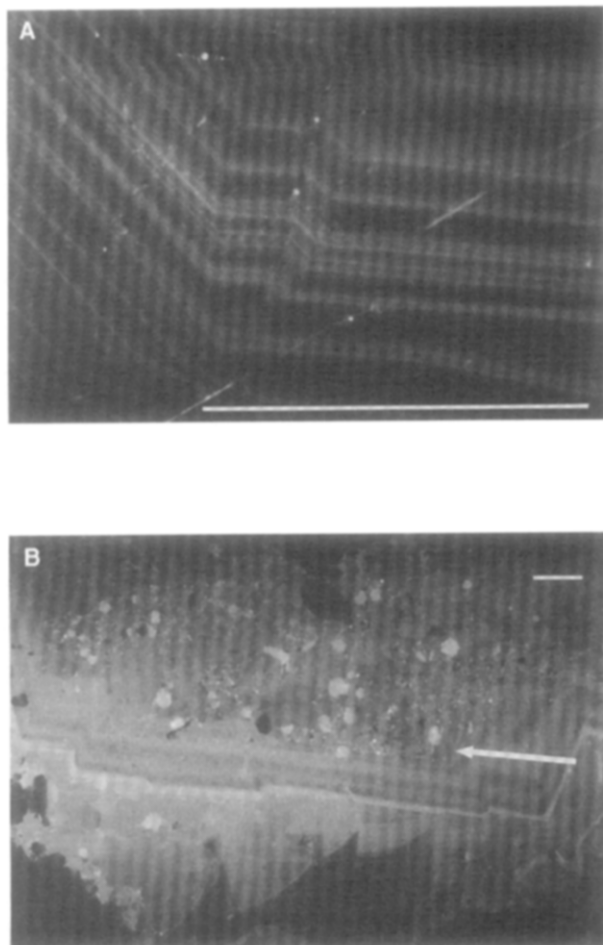
Fig. 4 (a) Photomicrograph of fine-scale luminescent zoning characteristic of calcites from the upper unsaturated zone. Scale bar is 100 μm. (b) Photomicrograph exhibiting broader-scale luminescent zoning (center of image) found in many carbonate-altered zone calcites. Arrow points to boundary between tuff (patchy area above arrow) and calcite (zoned area below arrow). Scale bar is 200 μm.

of luminescent bands reflecting differing plane slices through calcite cross-sections. Unambiguous discontinuities, such as dissolution boundaries, exist in only a limited number of samples (Fig. 5).

5.2. Minor and Trace Element Chemistry of Calcite

5.2.1. Manganese, iron, and strontium

Electron microprobe and SIMS analyses of Yucca Mountain calcite corroborate bulk analyses in that minor and trace element abundances generally distinguish shallow calcrete and calcite from the UUZ, BZ, and CAZ (Table 1). Manganese abundances appear particularly representative, while Sr and Fe concentrations overlap substantially. As shown in Fig. 6, the majority of calcite minor element abundances plot in two fields, one Mn-enriched and the other Mn-depleted, contrasting most CAZ samples with shallower occurrences.

While minor element concentrations remain consistent enough between samples to allow correlations to location within Yucca Mountain, Mn, Fe, and Sr abundances nonethe-

less vary considerably within most individual calcites. Variations in trace element concentrations within single UUZ calcites are as large as 0.41–13.0 ppm for Mn (L1896), 15.2–200 ppm for Fe (L49), and 5.60–167 ppm for Sr (L770). CAZ calcite range from approximately 1250–29,500 ppm for Mn (L262), 84–2050 ppm for Fe (L261), and 154–2000 ppm for Sr (L262) (Table 1).

As shown in previous studies (Long and Agrell, 1965; Mason, 1987), Fe and Mn abundances fluctuate according to the luminescence of individual zones, with luminescing zones typically high in Mn and low in Fe, and nonluminescing zones the reverse. Luminescent zonation must be considered, therefore, when interpreting Mn and Fe distributions within individual calcite samples. However, no identifiable trends were observed between Mn, Fe, or Sr in luminescent zones and distance from the fracture wall. The only observable trend is that the earliest phases of calcite are typically the most enriched in these minor elements.

Of the eighteen samples analyzed in this study, one contains isotopic signatures inconsistent with its present environment. Minor element abundances in UUZ sample L769 are similar in abundance to other UUZ calcite samples, but average $\delta^{13}C = 2.7$ and $\delta^{18}O = 16.3$ (SMOW) values suggest an affinity to CAZ calcite (Whelan et al., 1994). A second sample, BZ calcite L772, was collected from the present saturated zone and yet exhibits the low (sub-ppm) minor element abundances typical of UUZ calcite values. Isotopically, however, L772 is not anomalous with respect to model calcite compositions that would precipitate from existing Yucca Mountain groundwater (Whelan and Moscati, unpubl. data).

5.2.2. REE distributions

Data obtained using SIMS reveal distinctions in REE fractionation between CAZ and BZ/UUZ calcites similar to those observed using bulk chemical analysis methods (Vaniman, 1993). Chondrite-normalized REE patterns for calcite analyzed in this study are shown in Fig. 7. The presence of a prominent negative Ce anomaly and a pronounced negative Eu anomaly distinguish UUZ calcite from the flat Ce pattern and minimal negative Eu anomaly associated with CAZ occurrences.

In addition, SIMS analyses reveal previously unseen light rare earth element (LREE) depletion in some growth zones. As a result, four general types of REE pattern may be defined in Yucca Mountain calcite, using the following ratios based on chondrite-normalized data: (1) depleted LREE (La/Sm ~ 1) with pronounced negative Ce (La/Ce ~ 200) and Eu (Sm/Eu ~ 10) anomalies, (2) enriched LREE (La/Sm > 2) with pronounced negative Ce (La/Ce ~ 700) and Eu (Sm/Eu ~ 20) anomalies, (3) depleted LREE (La/Sm ~ 1), with a small Eu (Sm/Eu ~ 3) anomaly and a minimal Ce anomaly (La/Ce ~ 0.5), and (4) enriched LREE (La/Sm ~ 6) with a small Eu (Sm/Eu ~ 2) anomaly and a minimal to nonexistent Ce (La/Ce ~ 1.5) anomaly (Fig. 8).

REE abundances vary considerably within individual samples. As with Mn and Fe, REE distributions appear closely tied to luminescent zonation. Unlike Mn and Fe, however, zones of similar luminescence typically decrease in REE
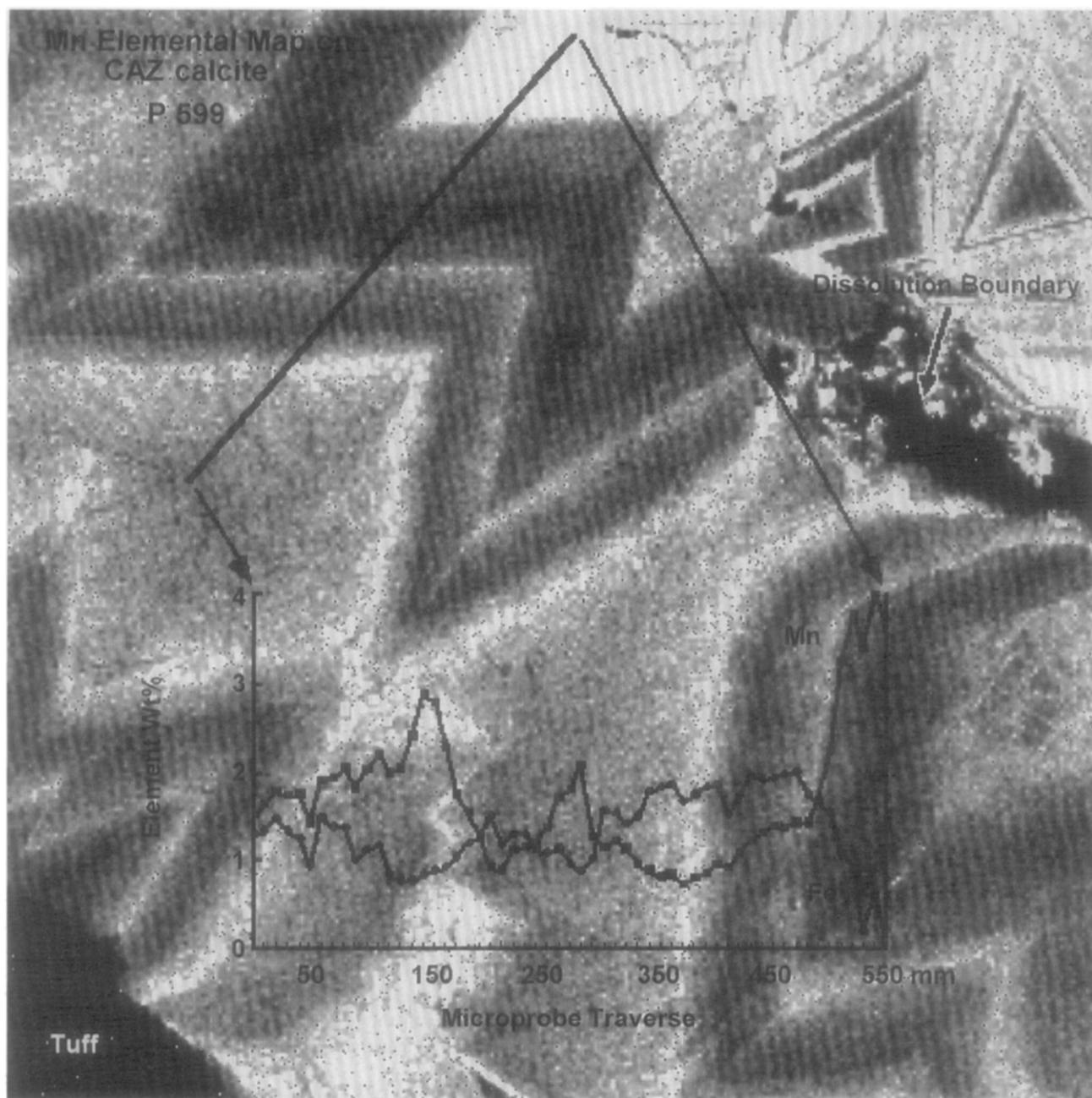
Fig. 5. Electron microprobe elemental image for Mn correlated with Mn and Fe abundances from a linear traverse across luminescing and nonluminescing zones. Note the change in zone size on opposing sides of the dissolution boundary in the upper right-hand corner.

abundance with distance from the fracture wall. A concomitant decrease in CL intensity with distance away from the fracture wall is not observed, however.

While the REE concentrations vary considerably among growth zones within individual samples, chondrite-normalized REE patterns remain internally consistent. Calcite samples exhibiting a negative Ce anomaly in luminescing growth zones also have negative Ce anomalies in associated nonluminescing zones. The only pronounced deviations appear to be artifacts of LREE depletion. These differences are evident in CAZ samples L262 and L599 and are due to lower La

and Ce abundances in some growth zones (e.g., analyses 2 and 6, L599; Fig. 7b). In UUZ and BZ samples, La/Ce ratios are highly variable and do not appear to change systematically within individual samples (Fig. 7a,b).

REE relative concentrations illustrate the similarities between UUZ and BZ calcites. The BZ sample, L772, collected below the water table, has pronounced negative Ce (La/Ce = 200) and Eu (Sm/Eu = 26) anomalies that are similar to UUZ calcite (same anomaly seen in INAA data; Vaniman, 1994). La/Sm = 2 for L772 is also equivalent to UUZ occurrences. In addition, luminescence in L772 is predomi-
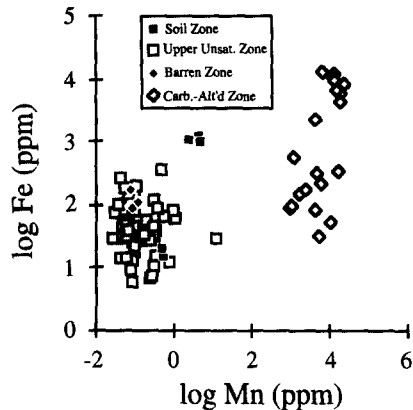
Fig. 6. Plot of Fe vs. Mn for Yucca Mountain calcite samples determined using SIMS. Note the clustering of points associated with individual samples as well as with relation to the water table. Note the Mn-abundance gap between UUZ and CAZ samples.

nantly composed of the small-scale concentric zoning characteristic of UUZ calcite. REE concentrations obtained from the isotopically anomalous UUZ sample L769, however, do not clearly distinguish it from other UUZ calcite. Chondrite-normalized REE patterns derived from SIMS analyses of this sample reveal a pronounced negative Ce anomaly similar in relative magnitude to associated, stratigraphically similar secondary carbonates (Fig. 7a). INAA analysis of L769 also reveals the presence of a negative Ce and Eu anomaly, although this method suggests that Ce depletion is minimal relative to those determined using SIMS (Vaniman and Chipera, 1996).

5.3. Manganese Oxides

Analyses of NBS Mn standard GXR-3 and three manganese oxide mineral separates from Yucca Mountain were performed using ICP-MS (Table 2). Samples are composed predominantly of manganese oxide phases with varying amounts of impurities (quartz, tridymite, feldspar, hematite, and smectite). The three manganese oxide mineral separates were: (1) cryptomelane (KMn_8O_{16}), with minor ($<25\%$) todorokite (($Mn,Ca,Mg)Mn_3O_7 \cdot H_2O$) and smectite, collected in the saturated zone from borehole G-4, (2) lithiophorite (($Mn_5^{4+}Mn^{2+}O_{12})(Al_4Li_2(OH)_{12})$), with major ($>50\%$) smectite and quartz, minor tridymite, feldspar, and hematite, and trace ($<5\%$) rancieite (($Ca,Mn^{2+})Mn_4^{4+}O_9 \cdot 3H_2O$), collected near the water table in borehole GU-3, and (3) rancieite with major smectite and trace hematite, that was obtained from the unsaturated zone in borehole G-2. Chondrite-normalized patterns for these samples are shown in Fig. 9. The REE pattern of the cryptomelane sample (MnG4) is LREE enriched with a small negative Eu (Sm/Eu = 3) anomaly, while the lithiophorite-rich sample (MnGU3) is REE enriched (La = 1700 ppm) with a negative slope (La/Lu) = 2 and a pronounced negative Eu anomaly (Sm/Eu > 700), and the rancieite-rich sample (MnG2) has a slightly positive REE slope (La/Lu = 0.75) and a substantial positive Ce anomaly (La/Ce = 0.1).

6. DISCUSSION

It is important to remember that all interpretations of trace element data in settings such as Yucca Mountain are to some extent compromised by the lack of understanding of trace element partitioning between aqueous solutions and carbonates at low temperatures. Numerous experimental studies testify to this point (Graf, 1988; Terakado and Masuda, 1988; Zhong and Mucci, 1995). Nevertheless, trace element characteristics of the Yucca Mountain calcite allow us to gain additional perspectives concerning (1) the nature and origin of the trace element signatures within calcite that precipitated under different ground water conditions at Yucca Mountain and (2) the variations in trace element systematics during calcite growth and its possible reflection of changing precipitation conditions.

6.1. Minor and Trace Elements as Fingerprints for Crystallization Conditions

The different trace element characteristics distinguishing soil zone, UUZ, and CAZ calcites, as well as differences in trace element abundances within individual samples, provide a means of distinguishing processes of calcite precipitation, trace element incorporation into calcite, and conditions of calcite crystallization. At least three possible mechanisms may be responsible for the origin of REE patterns (Ce and Eu anomalies, REE abundance, and REE pattern slope) and minor element (Fe, Mn, Sr) characteristics in calcite. Since understanding the origin of the negative Ce anomaly in UUZ calcite is a critical first step in applying it as a fingerprint of changing calcite crystallization conditions, the following is a discussion of three mechanisms that may be responsible for its formation.

6.1.1. Model I: Kinetic and structural controls of cerium fractionation

The calcite structure can be described in terms of a derivative of the NaCl structure in which CO_3 groups replace the Cl, and Ca is in place of Na. The CO_3 groups cause the resulting structure to be rhombohedral rather than isometric. The CO_3 groups lie in planes at right angles to the three-fold (c) axis and the Ca ions lie in alternating planes. The Ca ions are in sixfold coordination with the O of the CO_3 groups forming a slightly distorted octahedron. Within a given layer, the octahedra are independent, sharing neither edges nor corners. Adjacent octahedra are linked by CO_3 and through the corners of octahedra from layers above and below. Each O is coordinated to two Ca ions as well as to a C ion at the center of the CO_3 group (Klein and Hurlbut, 1985). Trace elements documented in this study will only substitute into the octahedrally coordinated Ca site. Parameters describing the Ca site characteristics in calcite can be calculated based on the methods used by Smyth and Bish (1988), Caporuscio and Smyth (1990), and Shearer and Larsen (1994). Using data of Smyth and Bish (1988), the optimal cation site radius, site electrostatic potential, and the optimal cation charge for the Ca site in calcite may be calculated. The REE having the valence and ionic radius closest to these optimal site characteristics will be preferred

a

Upper Unsaturated Zone Calcites
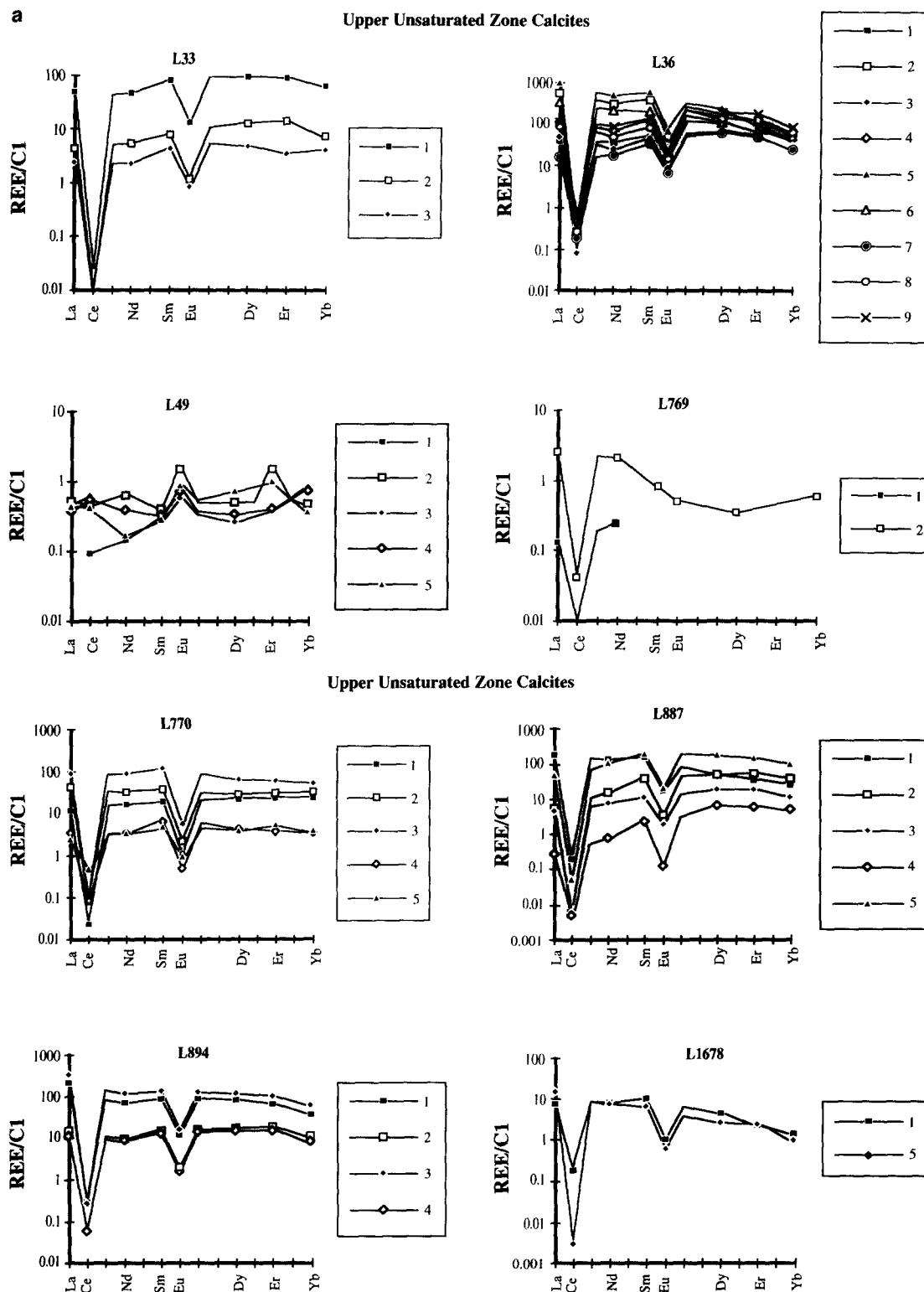

Upper Unsaturated Zone Calcites

Fig. 7. Chondrite-normalized REE patterns of Yucca Mountain calcites. REE pattern numbers are the same as analysis numbers in Table 1.

(Table 3). Therefore, based solely on these constraints, middle and heavy rare earth elements (HREE) should be preferentially enriched in calcite relative to the LREE.

While most lanthanides are trivalent, waters that are oxidizing or extremely alkaline may transform Ce^{3+} to Ce^{4+} (Brookins, 1989). The ionic radius of Ce^{4+} ($I = 0.88$ Å) is

Upper Unsaturated Zone Calcites

b   Barren Zone & Carbonate-Altered Zone Calcites
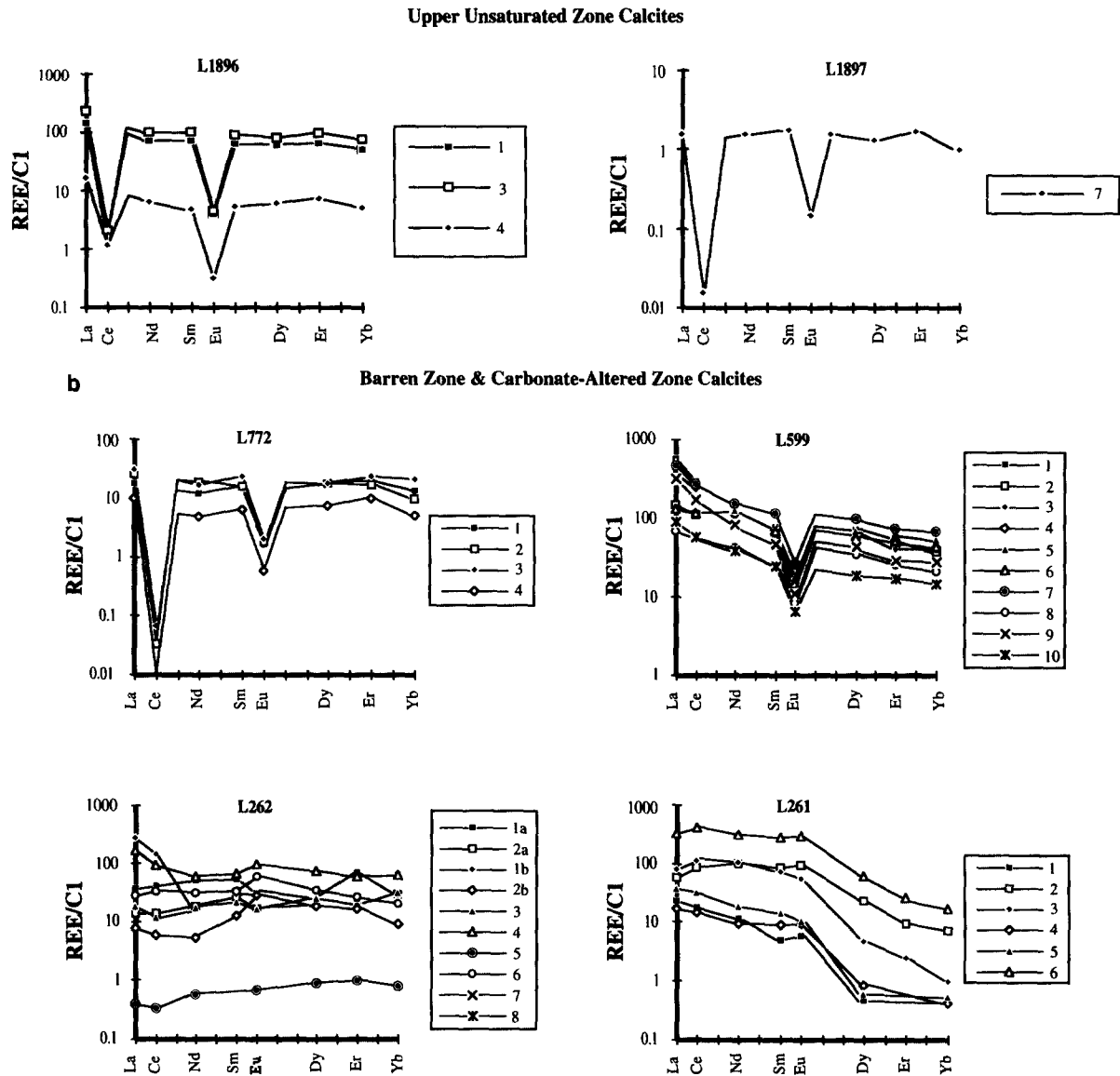
Fig. 7. (Continued)

very small, resulting in a cation closer in size to the HREE than to the LREE. Based on differences in ionic radii, two potential mechanisms may explain the negative Ce anomaly typical of UUZ calcite. First, during calcite precipitation, conditions in the unsaturated zone may have been oxidizing enough to form Ce^{4+} while relatively reducing conditions in the saturated zone stabilized Ce^{3+}. In this case, size or charge constraints may have excluded Ce^{4+} from unsaturated zone calcite, while calcite crystallizing in the saturated zone incorporated the larger Ce^{3+} along with the other trivalent REE.

Differences between the ionic valences and radii of Ce^{4+} and the REE^{3+} do not readily address other chemical variations within individual calcite samples. UUZ sample L36, for instance, contains both low La/Yb and high La/Yb growth zones. As previously discussed, these differences in relative REE abundance cannot be readily accounted for by changes in solution Eh/pH.

6.1.2. Model II: Different trace element sources

A second possible mechanism for establishing the pronounced negative Ce anomaly is that the REE included in UUZ calcite were derived from a different source(s) than CAZ samples. Since the host solutions of UUZ calcite are believed to be infiltrating surface waters, one logical source to consider is the soil zone and associated surficial materials such as eolian carbonate deposits. If REE were weathered from near-surface calcite, then REE abundances might be expected to decrease with depth, in which case soil zone calcite would exhibit higher REE enrichment than UUZ calcite. As previously discussed, this decrease in REE abundance with depth is not observed. The REE patterns (excluding Ce anomalies in UUZ calcite) in both unsaturated zone and saturated zone calcites closely emulate the REE patterns of the host tuffs (Fig. 10), suggesting that REE are derived
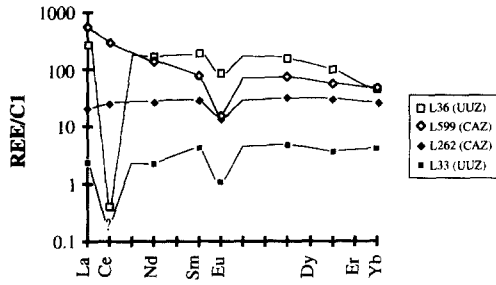
Fig. 8. Graph illustrating the four general REE patterns observed in Yucca Mountain calcites using SIMS. "?" refers to variability of Ce depletion throughout and among samples.

locally, and the similarity in REE and other trace elements between the BZ and UUZ calcites suggests common sources for these elements in both environments (e.g., volcanic glass sources for REE; see Vaniman and Chipera, 1996).

As previously discussed, the majority of CAZ calcite probably crystallized from hydrothermal solutions approximately 200°C warmer than UUZ calcite-depositing solutions. Little evidence is available, however, to suggest that the differences in these solution temperatures is responsible for the differences in calcite REE chemistry (i.e., Ce depletion in UUZ samples). Although little is known about REE behavior in hydrothermal solutions, Graf (1988) suggests that solution temperatures do not change the internal relationships among REE distribution coefficients.

6.1.3. Model III: Effects of co-precipitating/pre-precipitating phases on trace element distributions

In many of the manganese oxides identified in fractures at Yucca Mountain, the Mn site is in VI-coordination (Burns

Table 2. Results of quantitative (REE) and semi-quantitative (Y, Pb, Th, and U) ICP-MS analyses of select MnO separates. GXR3 = NBS Mn-oxide standard; G-4, GU-3, and G-2 = Yucca Mt. samples (see text for mineral i.d. and abundance estimates of individual phases). GXR3* = values reported by NBS (Govindaraju, 1989). NA = not available. Data in ppt.

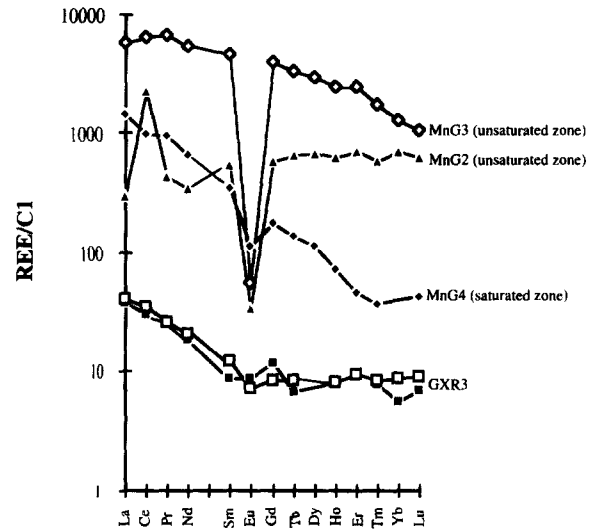|	GXR-3*	GXR-3	MnG4	MnGU3	MnG2
La	8.8	6.9	590	1700	94
Ce	18	18	1100	6000	2100
Pr	NA	2.3	160	840	60
Nd	8.3	7.6	440	2500	190
Eu	0.48	1.3	11	4.7	4.5
Sm	1.3	4.1	110	890	110
Gd	2.3	11	100	370	55
Tb	0.24	0.4	10	160	31
Dy	NA	1.8	34	690	160
Ho	NA	0.5	8.2	190	46
Er	NA	1.6	26	550	150
Tm	0.19	0.2	3.7	63	23
Yb	0.91	1.2	21	240	110
Lu	0.17	0.2	3.4	36	20
Y	15	21	140	6700	1400
Pb	15	34	760	2400	1500
Th	2.9	5.3	110	330	120
U	3.0	4.4	65	57	5.9

Fig. 9. Chondrite-normalized REE patterns of Yucca Mountain manganese oxides. Data from ICP-MS analyses. Oxide phases are: MnG4 = cryptomelane (with minor todorokite and smectite); MnGU3 = lithiophorite (with major smectite and quartz, minor tridymite, feldspar, and hematite, and trace rancieite); MnG2 = rancieite (with major smectite and trace hematite). NBS values for GXR3 are represented by filled squares.

and Burns, 1979). Manganese occurs in a variety of valences in manganese oxides at Yucca Mountain, but some is present as Mn^{2+}. The similar size of VI-coordinated Ce^{4+} ($I = 0.80$ Å) and Mn^{2+} ($I = 0.82$ Å) facilitates scavenging of Ce^{4+} by co-precipitating manganese oxides, while Ce^{3+} ($I = 1.034$ Å in VI coordination) is too large to substitute readily for Mn^{2+}. This crystal chemical mechanism for fractionating Ce from other REE has been documented in marine manganese nodules by Piper (1974), Elderfield et al. (1981), and de-Baar et al. (1988). Scavenging of Ce by contemporaneously precipitating fracture-lining manganese oxides such as crypt-

Table 3. Ionic radii and valences for elements of interest in this study. OSC = optimal site characteristics (Smyth and Bish, 1988). Data from Shannon and Prewitt (1969).

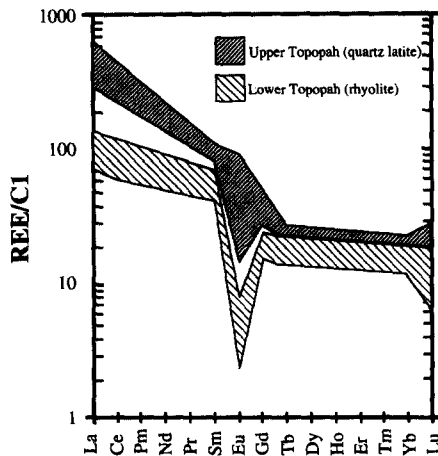| Element	Valence	VI-Coord. Radius (Å)
Ca	2+	1.00
Sr	2+	1.16
Mn	2+	0.82
Mn	4+	0.54
Fe	2+	0.77
Fe	3+	0.645
La	3+	1.016
Ce	3+	1.034
Ce	4+	0.88
Nd	3+	0.995
Sm	3+	0.964
Eu	2+	1.17
Eu	3+	0.95
Dy	3+	0.908
Er	3+	0.881
Yb	3+	0.858
OSC	1.99+	0.96

Fig. 10. Ranges in chondrite normalized REE patterns for upper and lower portions of the Topopah Spring Tuff. After Schuraytz et al. (1989) and Broxton et al. (1989).

omelane, pyrolusite, and todorokite and/or associated phases (clays) has been proposed as a mechanism responsible for REE fractionation in Yucca Mountain calcite (Vaniman, 1993). Although it is difficult to constrain the exact mechanism responsible for incorporation of Ce into these manganese oxide phases, two are proposed here. First, if Ce^{4+} had been stable only in the relatively oxidizing conditions of the unsaturated zone, then (1) in the unsaturated zone, the similar ionic radii of VI-coordinated Ce^{4+} and VI-coordinated Mn^{2+} would have facilitated uptake of Ce by manganese oxide phases, and (2) in the saturated zone, ionic radii of VI-coordinated Ce^{3+} and VI-coordinated Mn^{2+} in manganese oxides would not have fractionated Ce from the other REE in calcite. Second, if both saturated and unsaturated zones were equally oxidizing during periods of calcite and manganese oxide precipitation, the substantially larger volumes of water and the higher fluid/rock interaction in the saturated zone might have diluted the importance of Ce-scavenging by manganese oxides. Evidence for the latter argument may lie in the diminished negative Ce and Eu anomalies in L772 (as determined by INAA), although some uncertainty is caused by discrepancies between SIMS and INAA analyses. However, while the $\delta^{18}O$ isotopic composition of L772 is in line with oxygen isotopic values modeled from current groundwater and may represent recent calcite precipitation, the similarity in CL zoning between L772 and UUZ calcite may suggest that this sample was precipitated under conditions similar to UUZ occurrences.

ICP-MS analyses of several manganese oxide phases associated with calcite in fractures at Yucca Mountain yield a wide range of REE patterns (Fig. 9). Sample MnG4, composed predominantly of cryptomelane with minor todorokite and smectite, exhibits considerable LREE enrichment and has no noticeable Ce enrichment, whereas the MnG2 sample with rancieite, major smectite, and trace hematite has a pronounced positive Ce anomaly (La/Ce = 0.15). The fact that the sample with a positive Ce anomaly was collected from the unsaturated zone suggests the possibility that Ce^{4+} was stable only in the unsaturated zone; alternatively, rancieite

may be much more effective in scavenging Ce^{4+} than cryptomelane and lithiophorite.

The enrichment of LREE in manganese oxide minerals without Ce anomalies suggests that these phases may play a role in the depletion of the LREE from unsaturated zone calcite and from a limited number of saturated zone calcite samples. In addition to explaining differences in trace element chemistries among samples, this model provides the most straightforward mechanism by which to account for variations in LREE/HREE ratios within individual calcites. Vaniman and Chipera (1996), noting the similarity in REE pattern slopes between secondary carbonates and their host tuffs, suggest that REE in secondary carbonates might be locally derived. Although the limited number of samples analyzed in this study do not allow such a comparison, the variations in LREE slopes observed within individual calcites may suggest that manganese oxide scavenging plays an important role in determining temporal changes in REE distribution or that the REE chemistry of calcite precipitating solutions may have changed through time due to the introduction of fluids which had interacted with different lithologies. In addition, observed manganese oxide/calcite abundance ratios determined by Carlos et al. (1993) lie within predicted values based on mass balance calculations (Denniston, 1995).

The co-existence of Ce and Eu anomalies in these calcite samples is not problematic, as the Eu anomaly is clearly inherited from the tuffaceous host rocks. However, the enhanced depletion of Eu along with Ce in many unsaturated zone samples is puzzling. The ionic radius of Eu^{2+} (1.25 Å in VI coordination) is almost identical to that of Sr^{2+} (1.21 Å in VI coordination). However, no systematic relationship exists between Eu and Sr in Yucca Mountain calcite. This may suggest that Eu and/or Sr is also being incorporated into other secondary mineral phases or that Eu and Sr are derived from different sources. Semiquantitative ICP-MS analyses reveal that in addition to Ce, manganese oxides or their associated phases are also enriched in Sr and Ba. For instance, manganese oxide sample MnG4 contains approximately 1% Sr and 5% Ba. Other secondary minerals at Yucca Mountain also exhibit a variety of REE patterns with abundances similar to calcite, with La values ranging from 2 to 90 × chondrite. Separates of opal, palygorskite, and fluorite from Yucca Mountain fracture systems have negative Ce anomalies, like the associated calcite (Vaniman and Chipera, 1996). It appears, therefore, that the mechanisms leading to negative Ce anomalies in calcite affect these minerals as well.

While Ce-scavenging by manganese oxide phases appears to be a reasonable model for explaining Ce-depletion in unsaturated zone calcite, Carlos et al. (1993) note that manganese oxide phases typically underlie calcite deposits along fractures, although pyrolusite intergrown with calcite has been found as well (Vaniman and Chipera, 1996). If most manganese oxides predate fracture-lining calcite and are responsible for the negative Ce anomaly in UUZ calcite, then existing manganese oxides may deplete infiltrating solutions of Ce by cation exchange prior to calcite crystallization. The observation that Ce is not depleted to the same extent in growth zones from individual UUZ calcite samples suggests

that either calcite is precipitating from solutions with distinct REE chemistries or that fluid chemistries are consistently being modified during calcite crystallization.

In summary, it appears that trace element abundances in Yucca Mountain calcite reflect the location of their crystallization (soil zone, UUZ, CAZ). Although only a limited number of samples were analyzed in this study, the shape of chondrite-normalized REE patterns in calcite likely reflects fluid-rock interaction with the adjacent, host tuffs. If this is true, the REE pattern of the calcite is locally controlled. Although overall pattern shape and the extent of the Eu anomaly may be controlled by the equilibrium between fluids and local tuff lithologies, scavenging by manganese oxide phases, particularly rancieite, appears to be an important factor in controlling the behavior of Ce in the calcite. Growth of manganese oxides may also be responsible for variations in LREE among growth zones in individual samples. Therefore, overall pattern shape may be controlled by a number of interacting variables such as which manganese oxide assemblage is stable, the Ce^{4+}/Ce^{3+} ratio in the solution, and the REE characteristics of the adjacent country rock and associated fluid. The overall concentration of REE (and other trace elements) in the calcite is attributed to both their concentration in the solution and the crystallization kinetics incorporating them into the calcite structure.

6.2. Compositional Variations within Individual Calcite Samples

The observation that different growth zones within individual calcites exhibit similarly shaped, chondrite-normalized REE patterns suggests that either D_{REE} remain constant or that they all change by equal amounts. Within individual calcites, REE concentrations differ but overall REE patterns remain nearly parallel between zones, although there is, in some samples, a second-order variability in REE slopes within samples. Therefore, (1) Yucca Mountain calcite does not appear to have been noticeably influenced by dramatically different source waters, (2) mechanisms involved in changing REE incorporation into calcite do not fractionate the REE although Fe/Mn ratios change, and (3) changes in kinetics during crystallization of a calcite do not influence REE pattern shape.

7. CONCLUSIONS

This study reports the results of the development and application of a technique for analysis of REE and Sr, Mn, and Fe in calcite and dolomite by SIMS. From this work, the following conclusions are drawn.

Simultaneous analysis of Mn, Fe, Sr, and REE in carbonates by SIMS can be performed with a great deal of success. Low average detection limits (<ppm) for REE in Yucca Mountain calcite facilitate highly precise measurements within growth zones as narrow as 30 μm, with analytical precisions for REE between 2–10% and 5–15% at abundances of one hundred and ten times chondrite, respectively. This technique is complicated by the necessity of developing calibration curves for individual REE, the low ionization of REE in calcite and dolomite relative to most silicates, and the

difficulty of obtaining calcite standards which are chemically homogeneous with regards to trace and minor elements.

The consistency of the Ce anomaly fingerprint throughout growth zones of individual calcites, coupled with CL petrographic observations, seem to suggest that this calcite crystallized under conditions which did not change dramatically from start to finish. Unambiguous unconformities, such as dissolution surfaces, are few.

SIMS analyses of growth zones within individual calcites corroborate bulk chemical distinctions among soil zone, UUZ, BZ, and CAZ calcites noted by Vaniman (1993, 1994). Chemical heterogeneity is evident within individual samples, however, with wide ranges in REE abundance present within most calcite. Earlier (closer to tuff) phases are typically the most enriched in REE, and LREE-enriched and LREE-depleted growth zones are common within individual samples. In addition, adjacent growth bands will have dramatically different concentrations of REE, Sr, Fe, and Mn. These observations suggest that either the concentrations of these elements in the solutions fluctuated during calcite precipitation or changes in conditions of crystallization (i.e., growth rate) or other kinetic factors (i.e., partitioning associated with luminescent banding) may have affected how the trace elements are incorporated into calcite.

Despite considerable chemical heterogeneity, the shape of chondrite-normalized REE patterns remains internally consistent, implying that conditions of precipitation or mechanisms of REE incorporation did not change radically during calcite growth. For example, if REE distribution coefficients change during calcite precipitation, they changed uniformly. Slight distinctions in LREE abundances between growth zones in individual calcites may reflect mixing of different solutions, or they may be derived from kinetic phenomena. However, the apparent degree of Ce fractionation (expressed as La/Ce ratios) appears to change nonuniformly among growth zones.

Scavenging by manganese oxide phases, particularly rancieite, appears to be an important factor in forming the negative Ce anomalies characteristic of UUZ calcite. Manganese oxides may also be responsible for variations in LREE among growth zones in individual samples. The specific mechanism responsible for trace element incorporation into these phases is still unclear, but REE distributions in calcite suggest that scavenging occurred from the fluid prior to calcite crystallization, probably by cumulative exposure to manganese oxides along flow paths.

Cathodoluminescence patterns, electron microprobe data, and SIMS analyses agree with the results of bulk chemical (INAA) analyses of calcites. Therefore, trace element abundances and REE patterns in calcite appear to reflect the location of calcite precipitation (soil zone, UUZ, CAZ).

REFERENCES

Bathurst R. G. C. (1975) *Carbonate Sediments and Their Diagenesis.* Elsevier.

Bish D. L. and Aronson J. L. (1993) Paleogeothermal and paleohydrologic conditions in silicic tuff from Yucca Mountain, Nevada. *Clays Clay Minerals* **41**, 148–161.

Bish D. L. and Chipera S. J. (1989) Revised mineralogic summary of Yucca Mountain, Nevada. Los Alamos Nat. Lab. Rept. LA-11497-MS.

Broad W. J. (1990) A mountain of trouble. *New York Times Magazine,* Nov. 18, 1990.

Brookins D. G. (1989) Aqueous geochemistry of rare earth elements. In *Geochemistry and Mineralogy of Rare Earth Elements* (ed. B. R. Lipin and G. A. McKay), Vol. 21, pp. 201–225. MSA.

Broxton D. E., Warren R. W., and Byers F. M. (1989) Chemical and mineralogical trends within the Timber Mountain-Oasis Valley caldera complex, Nevada: Evidence for multiple cycles of chemical evolution in a long-lived silicic magma system. *J. Geophys. Res.* **94**, 5961–5985/Appendix.

Burns R. G. and Burns V. M. (1979) Manganese Oxides. *Rev. Mineral.* **6**, 1–46.

Caporuscio F. A. and Smyth J. R. (1990) Trace element crystal chemistry of mantle eclogites. *Contrib. Mineral. Petrol.* **105**, 550–561.

Carlos B. A., Chipera S. J., Bish D. L., and Craven S. J. (1993) Fracture-lining manganese oxide minerals in silicic tuff, Yucca Moutain, Nevada, USA. *Chem. Geol.* **107**, 47–69.

Czarnecki J. B. and Waddell R. K. (1984) Finite-element simulation of groundwater flow in the vicinity of Yucca Mountain, Nevada-California. U.S. Geol. Surv. Water-Res. Invest. Rept. 84-4349.

deBaar H. J. W., Greman C. R., Elederfield H., and Van Gaans P. (1988) Rare earth element distributions in anoxic waters of the Cariaco Trench. *Geochim. Cosmochim. Acta* **52**, 1203–1220.

Denniston R. F. (1995) Trace and minor element distributions in fracture calcites from Yucca Mountain, Nevada: Reconstructing calcite growth histories. M. S. thesis., Univ. New Mexico.

Denniston R. F., Gauerke E., Shearer C. K., Vaniman D. T., and Hickmott D. (1993) Trace element distributions in fracture calcites from Yucca Mountain, Nevada: Implications for shallow crustal transport phenomena. *Eos* **74**, 677 (abstr.).

Denniston R. F., Shearer C. K., and Vaniman D. T. (1994a) Application of cathodoluminescence and minor-trace element micro-analysis for deciphering the crystallization history of calcite from shallow crustal regimes. *Eos* **75**, 371 (abstr.).

Denniston R. F., Shearer C. K., and Vaniman D. T. (1994b) An ion microprobe study of trace element (REE, manganese, strontium) zoning in calcite from shallow crustal regimes. *Eos* **75**, 698.

Elderfield H., Hawkesworth C. J., Greaves M. J., and Calvert S. E. (1981) Rare earth element geochemistry of oceanic ferromanganese nodules and associated sediments. *Geochim. Cosmochim. Acta* **45**, 513–528.

Graf J. L. (1988) Partitioning behavior of rare earth elements between calcite and aqueous solutions at temperatures and salinities similar to those for ore fluids in Mississippi Valley-Type ore deposits. *Geol. Soc. Amer. Annu. Meeting Prog. Abstr.* Denver, A95–A96 (abstr.).

Govindaraju K., ed. (1989) Appendix I. *Geostandard Newsletter* **XIII,** Spec. Issue 3.

Hay R. L., Pexton R. E., Teague T. T., and Kyser T. K. (1986) Spring-related carbonate rocks, magnesium clays, and associated minerals in Pliocene deposits of the Amargosa Desert, Nevada and California. *Geol. Soc. Amer. Bull.* **97**, 1488–1503.

Klein C. and Hurlbut C. S., Jr. (1985) *Manual of Mineralogy.* John Wiley and Sons.

Long J. V. P. and Agrell S. O. (1965) The cathodoluminescence of minerals in thin sections. *Miner. Mag.* **34**, 318–326.

Mariano A. N. (1989) Cathodoluminescence emission spectra of rare earth element activators in minerals. In *Geochemistry and Mineralogy of Rare Earth Elements* (ed. B. R. Lipin and G. A. McKay), Vol. 21, pp. 339–348. MSA.

Marshall E. (1991) The geopolitics of nuclear waste. *Science* **251**, 864–867.

Mason R. A. (1987) Ion microprobe analysis of trace elements in calcite with an application to the cathodoluminescence zonation of limestone cements from the lower carboniferous of South Wales, U. K. *Chem. Geol.* **64**, 209–224.

Mason R. A. and Mariano A. N. (1990) Cathodoluminescence activation in manganese-bearing and rare earth-bearing synthetic calcites. *Chem. Geol.* **88**, 191–206.

Morse J. W. and Mackenzie F. T. (1990) *Geochemistry of Sedimentary Carbonates.* Elsevier.

Nickel E. (1978) The present status of cathodoluminescence as a tool in sedimentology. *Miner. Sci. Eng.* **10**, 73–100.

Peterman Z. E., Stuckless J. S., Marshall B. D., Mahan S. A., and Futa K. (1992) Strontium isotope geochemistry of calcite fracture fillings in deep core, Yucca Mountain, Nevada-a progress report. *Proc. 3rd Intl. High Level Rad. Waste Mgmt.,* 1582–1586.

Piper D. Z. (1974) Rare earth elements in ferromanganese nodules and other marine phases. *Geochim. Cosmochim. Acta* **38**, 1007–1022.

Quade J. and Cerling T. E. (1990) Stable isotopic evidence for a pedogenic origin of carbonates in trench 14 near Yucca Mountain, Nevada. *Science* **250**, 1549–1552.

Riciputi L. R., Cole D. R., Machel H. G., Christie W. H., and Rosseel T. M. (1992) Small scale trace element zonations in carbonates: An ion microprobe study of diagenesis in the Upper Devonian Nisku Formation, Western Canada Sedimentary Basin. In *Proceedings of the International Symposium on Water-Rock Interaction* (ed. Y. K. Kharaka and A. S. Maest), pp. 1197–1200.

Riciputi L. R., Machel H. G., and Cole D. R. (1994a) An ion microprobe study of diagenetic carbonates in the Devonian Nisku Formation of Alberta, Canada. *J. Sediment. Res.* **A64**, 115–127.

Riciputi L. R., McSween H. Y., Jr., Johnson C. A., and Prinz M. (1994b) Minor and trace element concentrations in carbonates of carbonaceous chondrites, and implications for compositions of coexisting fluids. *Geochim. Cosmochim. Acta* **58**, 1343–1351.

Roedder E., Whelan J. F., and Vaniman D. T. (1994) Fluid inclusion studies of calcite veins from Yucca Mountain, Nevada, tuffs: Environment of formation. *Proc. 5th Intl.Conf. High Level Rad. Waste Mgmt.,* 1854–1860.

Savard M. M., Veizer J., and Hinton R. (1995) Cathodoluminescence at low Fe and Mn concentrations: a SIMS study of zones in natural calcites. *J. Sediment. Res.* **A65**, 208–213.

Sawyer D. A., Fleck R. J., Lanphere M. A., Warren R. G., Broxton D. E., and Hudson M. R. (1994) Episodic caldera volcanism in the Miocene southwestern Nevada volcanic field: Revised stratigraphic framework, $^{40}Ar/^{39}Ar$ geochronology, and implications for magmatism and extension. *Geol. Soc. Amer. Bull.* **106**, 1304–1318.

Schuraytz B. J., Vogel T. A., and Younker L. W. (1989) Evidence for dynamic withdrawl from a layered magma body: The Topopah Spring Tuff, southwestern Nevada. *J. Geophys. Res.* **94-B5**, 5925–5942.

Shannon R. D. and Prewitt C. T. (1969) Effective ionic radii in oxides and fluorides. *Acta Cryst.* **B25**, 925–946.

Shearer C. K. and Larsen L. M. (1994) Sector-zoned aegirine from the Ilimaussaq alkaline intrusion, South Greenland: Implications for trace-element behavior in pyroxene. *Amer. Mineral.* **79**, 340–352.

Shimizu N., Semet M. P., and Allegre C. J. (1978) Geochemical applications for quantitative ion microprobe analysis. *Geochim. Cosmochim. Acta* **42**, 1312–1334.

Smyth J. R. and Bish D. L. (1988) *Crystal Structures and Cations Sites of the Rock-Forming Minerals.* Allen and Unwin.

Srinivasan K., Riciputi L. R, and Walker K. R. (1994) REE geo-

chemistry of Cambro-Ordivician platform carbonates: implications for sources of diagenetic fluids. *Geol. Soc. Amer. Fall Meet. Abstr. Progr.*, A-130.

Stuckless J. F., Peterman Z. E., and Muhs D. R. (1991) Uranium and strontium isotopes in ground water and calcite, Yucca Mountain, Nevada: Evidence against upwelling water. *Science* **254**, 551–554.

Swart P. K. (1990) Calibration of the ion microprobe for the quantitative determination of strontium, iron, manganese, and magnesium in carbonate minerals. *Anal. Chem.* **62**, 722–728.

Szabo B. J. and Kyser T. K. (1990) Ages and stable-isotope compositions of secondary calcite and opal in drill cores from Tertiary volcanic rocks of the Yucca Mountain area, Nevada. *Geol. Soc. Amer. Bull.* **102**, 1714–1719.

Terakado Y. and Masuda A. (1988) The coprecipitation of rare-earth elements with calcite and aragonite. *Chem. Geol.* **69**, 103–109.

Vaniman D. T. (1993) Calcite deposits in fractures at Yucca Mountain, Nevada. *Proc. 4th Intl. Conf. High Level Rad. Waste Mgmt.*, 1935–1939.

Vaniman D. T. (1994) Calcite deposits in drill cores USW G-2 and USW GU-3/G-3 at Yucca Mountain, Nevada. Los Alamos National Lab. Rept. LA-12720-MS.

Vaniman D. T. and Chipera S. J. (1996) Paleo-transport of lanthanides and strontium recorded in calcite compositions from tuffs at Yucca Mountain, Nevada. *Geochim. Cosmochim. Acta* **60**, 4417–4433.

Vaniman D. T. and Whelan J. F. (1994) Inferences of paleoenvironment from petrographic, chemical, and stable isotope studies of calcretes and fracture calcites. *Proc. 5th Intl. Conf. High Level Rad. Waste Mgmt.* 2730–2737.

Veizer J., Hinton R. W., Clayton R. N., and Lerman A. (1987) Chemical diagenesis of carbonates in thin-sections: Ion microprobe as a trace element tool. *Chem. Geol.* **64**, 225–237.

Whelan J. F. and Stuckless J. S. (1992) Paleohydrologic implications of the stable isotopic composition of secondary calcite within the Tertiary volcanic rocks of Yucca Mountain, Nevada. *Proc. 3rd Intl. Conf. High Level Rad. Waste Mgmt.* 1572–1581.

Whelan J. F., Vaniman D. T., Stuckless J. S., and Moscatti R. S. (1994) Paleoclimatic and paleohydrologic records from secondary calcite: Yucca Mountain, Nevada. *Proc. 5th Intl. Conf. High Level Rad. Waste Mgmt.* 2738–2745.

Zhong S. and Mucci A. (1995) Partitioning of rare earth elements (REEs) between calcite and seawater solutions at 25°C and 1 atm, and high dissolved REE concentrations. *Geochim. Cosmochim. Acta* **59**, 443–453.